JOURNAL OF SPACECRAFT AND ROCKETS
Vol. 30, No. 5, September–October 1993

Aerodynamic Heating Environment Definition/Thermal Protection System Selection for the HL-20

K. E. Wurster* and H. W. Stone*
NASA Langley Research Center, Hampton, Virginia 23681

Definition of the aerothermal environment is critical to any vehicle such as the HL-20 Personnel Launch System that operates within the hypersonic flight regime. Selection of an appropriate thermal protection system design is highly dependent on the accuracy of the heating-environment prediction. It is demonstrated that the entry environment determines the thermal protection system design for this vehicle. The methods used to predict the thermal environment for the HL-20 Personnel Launch System vehicle are described. Comparisons of the engineering solutions with computational fluid dynamic predictions, as well as wind-tunnel test results, show good agreement. The aeroheating predictions over several critical regions of the vehicle, including the stagnation areas of the nose and leading edges, windward centerline and wing surfaces, and leeward surfaces, are discussed. Results of predictions based on the engineering methods found within the MINIVER aerodynamic heating code are used in conjunction with the results of the extensive wind-tunnel tests on this configuration to define a flight thermal environment. Finally, the selection of the thermal protection system based on these predictions and current technology is described.

Nomenclature

h/h_0 = heat-transfer coefficient ratio
M_e = local Mach number
M_∞ = freestream Mach number
$\dot{q}/\dot{q}_{ref}$ = heat-transfer rate ratio
Re_θ = momentum-thickness Reynolds number
Re_∞ = freestream Reynolds number
x/L = axial location
z_e = postshock compressibility factor
ε = emissivity

Introduction

THE National Aeronautics and Space Administration has been examining vehicle concepts to complement the Space Shuttle system. These concepts would provide crew changeout capability at the Space Station Freedom, as well as other possible missions. The key objectives have been to provide an alternate manned access to space facilities and a safer, more reliable, cost-effective, and operationally efficient system for routine transportation of people to low Earth orbit. This system is referred to as the Personnel Launch System (PLS). The current configuration consists of a manned spacecraft or orbiter that would be launched by an expendable booster.

The Langley Research Center has been developing a lifting-body configuration called HL-20 for potential PLS orbiter application. This concept has been the subject of a detailed study that is described in several articles in this journal issue. Reference 1 presents an overview of the study. References 2–5 describe other aspects of the study critical to the determination of the aerodynamic heating environment for this vehicle. This article describes the approach used to estimate the aerothermal environment and the resulting predictions for the HL-20 vehicle. This approach combines analytical techniques with the results of several wind-tunnel tests that have been performed on this configuration. The thermal protection system (TPS) selection process is discussed as well, and several candidate systems are described.

Received Dec. 26, 1992; revision received Feb. 23, 1993; accepted for publication Feb. 25, 1993.

*Aerospace Engineer, Space Systems Division.

Typically, the approach to determine the aeroheating environment may range from a simplistic reference heating analysis to detailed computational fluid dynamics (CFD) analyses and actual flight tests. As the design process progresses, increasing levels of detail are required. In this study, work has progressed from the reference heating calculations, to engineering computations of the heating environments over several critical regions of the vehicle, and finally to several benchmark CFD solutions.[4] In addition, the results of many wind-tunnel tests are available.[6] This analysis procedure is believed to be unique in the field of preliminary design of aerospace vehicles. Generally, the aerothermodynamicist involved in the preliminary design of a configuration, such as HL-20, has not had the opportunity to compare results with either detailed CFD solutions or any, but the most rudimentary, wind-tunnel tests. Typically, this level of detail is reserved for the later stages of development.

Methodology

General Considerations

Prior to the determination of the vehicle heating environment, mission trajectories (ascent, abort, and entry) must be developed, and the critical flight conditions, which will design the TPS, must be determined. For a rocket-launched/lifting-entry vehicle such as

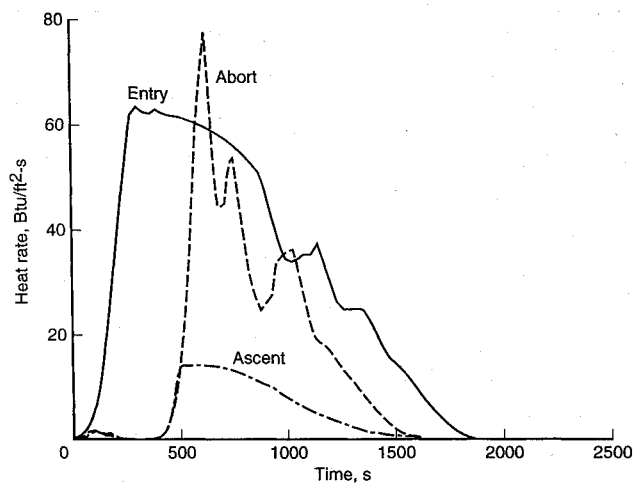

Fig. 1 HL-20 PLS stagnation heating-rate comparison: entry/abort/ascent

the PLS, the entry and abort will generally design the TPS. The TPS requirements are directly related to the heating rates and loads that the vehicle experiences. The peak heating rates determine the maximum temperatures and thus define the applicable TPS materials. The total heat load determines the corresponding insulation or active cooling requirements necessary to keep the structural temperatures within the material limits. An insulative TPS, such as the reusable surface insulation on the Shuttle, drives the trajectory design toward the higher heating-rate trajectories that tend to yield shorter entry times and lower heat loads, hence minimizing the TPS mass. A lower-temperature, radiative TPS, on the other hand, drives the trajectory design toward low heating rates and longer entry times with the resultant lower temperatures and higher heat loads. The higher heat loads are less significant since this type of system radiates a much greater percentage of the convective heat flux to the atmosphere than does an insulative system. For the purposes of this study, a heating-rate constraint was applied during the development of each of the trajectories such that temperatures would not exceed the capabilities of current or near-term passive TPS materials.

Figure 1 illustrates the stagnation-heating-rate time histories on the HL-20 vehicle for each of the potential TPS design phases; entry, ascent, and abort. Although the abort shows a peak heating level which exceeds that of either the entry or ascent, the entry was chosen as the design heating trajectory because it has a more sustained high-heating pulse. The primary concern on the abort was assumed to be vehicle and crew survivability. Although the heating spike might necessitate replacement of the nosecap and leading edges, it would not, in all likelihood, result in catastrophic failure of the vehicle. The corresponding heat loads are shown in Fig. 2, where it is clear that the entry will also determine the insulation requirements for the TPS. Thus, the entry case will be considered the design trajectory for the TPS, both in terms of material selection as well as insulation requirements.

After the design heating trajectory is determined, a series of engineering calculations are used to determine the aeroheating environment over several critical regions of the vehicle. Those regions include the stagnation areas of the nose and wing leading edges, windward centerline, leeward surfaces of the vehicle, and deflected control surfaces.

Analysis Tools

The aerodynamic heating analyses performed in this study include both engineering calculations using the MINIVER[7] code (MINIature VERsion of the JA70 aerodynamic heating code) and CFD calculations employing the LAURA[8] code (Langley Aerothermodynamic Upwind Relaxation Algorithm). The CFD calculations[4] were made at a few critical flow conditions and used primarily as benchmark cases for verification of the engineering results and secondarily for extrapolation of the engineering results to the remaining areas of the vehicle. In previous studies, comparisons of numerous in-house engineering and CFD predictions with Shuttle-Orbiter[9] and sphere-cone[10] flight- and wind-tunnel-test heating data, as well as comparisons with wind-tunnel heating data for advanced lifting-body concepts,[11] have validated the engineering techniques. The analyses, described next, utilize the engineering techniques incorporated in the MINIVER code.

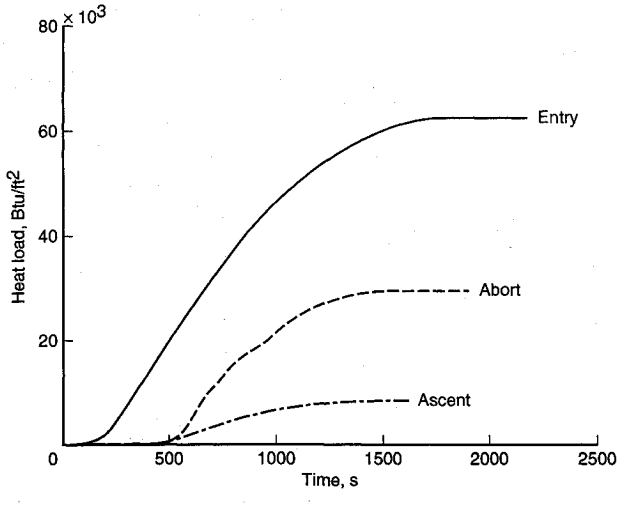

Fig. 2 HL-20 PLS stagnation heating-load comparison: entry/abort/ascent.

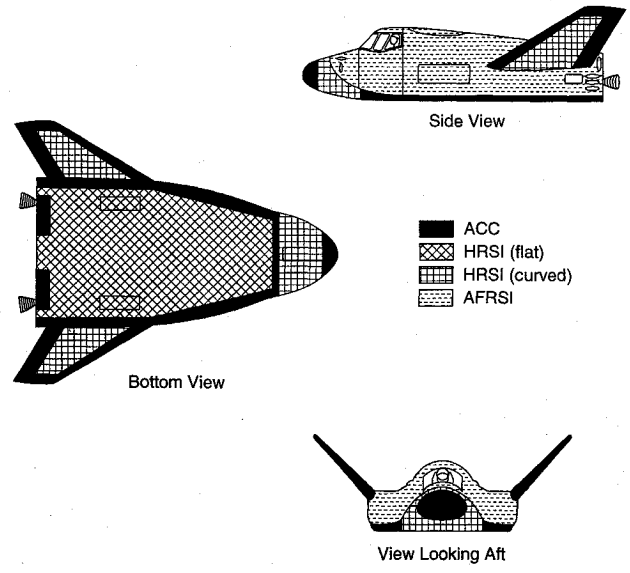

Fig. 3 HL-20 PLS thermal protection system.

MINIVER is a versatile engineering code that uses various well-known approximate heating methods, together with simplified flowfields and geometric shapes, to model the vehicle. Post-shock and local flow properties based on normal-shock or sharp-cone entropy conditions are determined in MINIVER through user selection of the various shock shape and pressure options. The calculations can be based on perfect-gas or equilibrium-air chemistry. Angle-of-attack effects are simulated either through the use of an equivalent tangent-cone or an approximate crossflow option.[12] The flow can be computed for two- or three-dimensional surfaces. However, the three-dimensional effects are available only through the use of the Mangler transformation[13] for flat-plate to sharp-cone conditions.

The primary advantage of the engineering code is the speed with which the analyses can be performed for each flow condition. This code allows determination of the critical aeroheating parameter time histories for a trajectory input directly from the Program to Optimize Simulated Trajectories (POST).[5,14] The time histories are critical to determination of the heat loads and thus the TPS insulation requirements. For conceptual or preliminary design, it is impractical to run the more detailed CFD solutions at a sufficient number of points in time to allow their use in determining TPS requirements.

The use of engineering codes, such as MINIVER, requires the engineer to have a "feel" for the flow environment over the vehicle being studied. As study of the HL-20 progressed, the results of several wind-tunnel tests were an invaluable aid in that process. Electron-beam flow visualizations and oil-flow test results[6] helped to determine the assumptions to be used in the MINIVER analyses. Those assumptions are described in the next section of this article. Although the MINIVER code predicts the heating environment only in certain regions of the vehicle, several aerothermal tests, including phase-change paint tests, infrared studies, and thermographic phosphor tests,[6,15] were used in conjunction with the benchmark CFD solutions to allow extrapolation of the MINIVER heating predictions to more general locations on the vehicle.

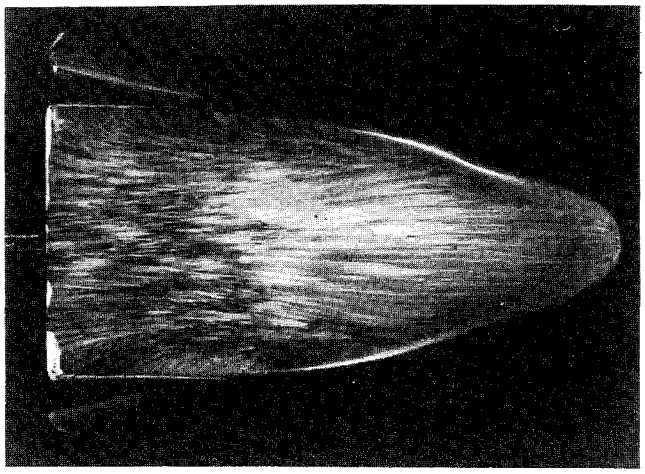

Fig. 4 HL-20 PLS oil flow patterns: Windward surface, Mach 6, angle-of-attack = 25 deg.

Assumptions

The engineering code requires a number of assumptions with regard to the flow environment and heating analysis. Two of the most critical of these, in terms of peak heating levels for this study, are 1) the assumption that the flowfield is dominated by blunt-body hypersonic flow, particularly on the windward surface, and 2) that there is no bow-shock impingement with the vehicle surface. Previous analyses[10] have shown that blunt-body effects dominate from 20 to 40 nose radii downstream. With an effective nose radius of well over 1 ft and a vehicle length of approximately 28 ft, this appears to be a reasonable assumption for the HL-20. The high angle-of-attack, 28.8 deg, at which the vehicle trims hypersonically results in a greater effective nose radius and virtually ensures the formation of a detached shock and the validity of the blunt-body assumption. Electron-beam flow visualizations have confirmed the existence of large shock-standoff distances and the absence of bow-shock impingement, at least at perfect-gas wind-tunnel conditions. However, the relatively high angle-of-attack also drives the recovery to sharp-cone conditions farther upstream on the vehicle. While the blunt-body assumption results in somewhat lower heating due to entropy effects, it will be shown later that the TPS material selections will be sufficiently conservative so that this assumption will not impact the results of this study.

Another assumption that has a very strong impact on the heating rates is the occurrence of transition to turbulent flow, since the turbulent heating rates are generally much larger than the laminar ones. The transition criteria chosen for this study were based on the ratio of the momentum-thickness Reynolds number to the local Mach number, Re_θ/M_e. Employing values extrapolated from Space Shuttle flight data,[16] we chose a value equal to 335 for Re_θ/M_e for transition onset and 415 for fully turbulent flow on the windward surfaces of the vehicle. The latter value results in fully turbulent flow occurring at roughly one and one-half times the distance to the onset of turbulence. Fully laminar flow was assumed on the nosecap and wing leading edges throughout the entry (continuum regime).

Nonequilibrium chemistry and finite-catalytic surface effects were not addressed in this study. Fully catalytic surfaces will yield higher heating rates due to dissociation and recombination at the surface. For this study, it was assumed that the TPS materials that ultimately will be used would have either low-catalytic characteristics, as do the silica-based ceramic tiles [High-temperature Reusable Surface Insulation (HRSI), Low-temperature Reusable Surface Insulation, Fibrous Refractory Composite Insulation (FRCI), High Thermal Performance (HTP), etc.] and the blanket materials [Advanced Flexible Reusable Surface Insulation (AFRSI), Tailorable Advanced Blanket Insulation, Composite Flexible Blanket Insulation, etc.] under consideration, or an applied low-catalytic surface coating such as the commercially available water-base, silica-alumina ceramic coating described in Ref. 17. A related assumption utilized in this investigation was that the surface emissivity, which represents the proportion of the incident heat radiated directly away to the atmosphere, could be maintained at a value roughly equal to 0.85. This number is considered typical of the ceramic materials in use today on the Space Shuttle Orbiter. Coatings might be necessary in order to maintain this emissivity value for multiple uses of the HL-20 vehicle.

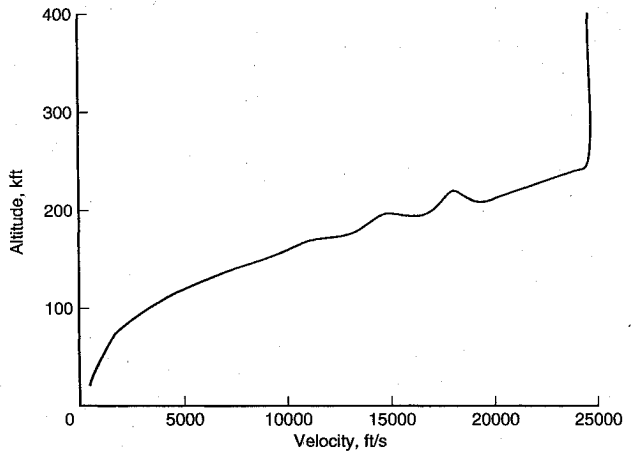

Fig. 5a Altitude-velocity profile for HL-20 PLS design entry trajectory: c.g. = 55.5%.

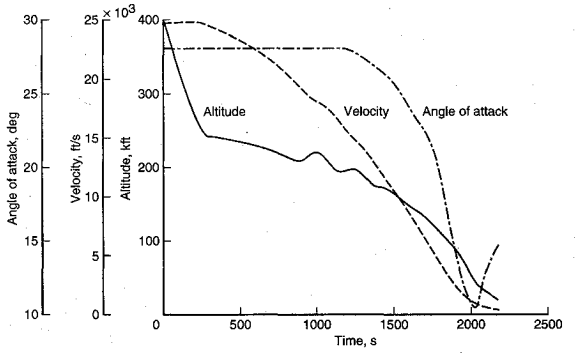

Fig. 5b Design entry trajectory parameter time histories for HL-20 PLS: c.g.= 55.5%.

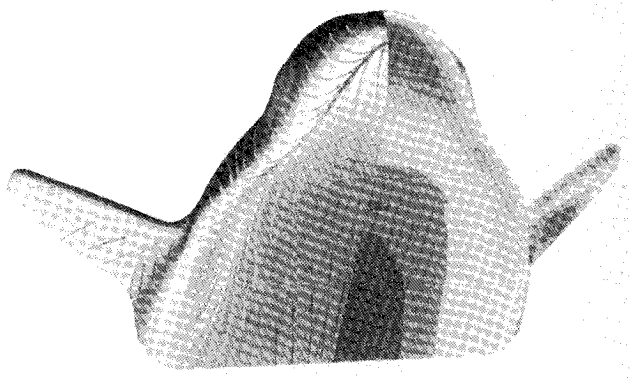

Fig. 6 HL-20 PLS equilibrium CFD solution-streamline/heating pattern: Mach 15.8, angle-of-attack = 25 deg.

Another important assumption involves the three-dimensional nature of the boundary layer on this vehicle. In this study, the Mangler transformation is used in the MINIVER code to transform the heating from that for a flat plate to that for a cone. Somewhat less obvious is the assumption of no crossflow. When crossflow occurs, the streamlines along the windward surface of a vehicle tend to diverge from the centerline. The boundary layer thins with increasing crossflow, and thus heating can be significantly higher when crossflow is present. Crossflow generally occurs anytime a three-dimensional circumferentially curved surface is inclined at an angle relative to the body angle. The HL-20 configuration, however, has a flat windward surface, as can also be seen in Fig. 3. Figure 4 illustrates the results of an oil-flow test at a 25-deg angle-of-attack for a Mach 6 wind-tunnel condition. The little streamline divergence that does occur is apparent primarily near the edges of the flat windward surface. Evidence, such as this, led to the assumption of zero crossflow for the present centerline calculations. In fact, Fig. 4 shows some evidence that inflow may occur near the centerline for this condition. This could actually reduce the heating slightly. Both the Mangler transformation and crossflow will have a much more significant impact on laminar heating than turbulent. It will be shown that laminar flow dominates during the peak heating phases of the entry, and thus, these assumptions will have a significant impact on the predicted heating levels in this study. Finally, the 1976 standard atmosphere,[18] together with the transport properties of Hansen,[19] and the tabulated thermodynamic properties from the Mollier chart for air,[20] are used in the code for determination of the appropriate properties in equilibrium air.

Entry Trajectory Development

The nominal design-reference-mission entry trajectory for the evaluation of the aerodynamic heating environment was developed using the POST program. The entry trajectory and guidance algorithm is described in Ref. 5.

During the entry phase, the vehicle enters the Earth's atmosphere at the trim angle of attack for undeflected control surfaces and maintains this attitude down to a Mach number of 3.5. The vehicle is initially in a heads-up, unrolled attitude. When the reference heating rate (stagnation-point heating to a 1-ft radius sphere as determined by Chapman's equation[21]) reaches a preselected value at pull-out, the vehicle is commanded to modulate the roll angle to maintain that heating rate without exceeding it. The heating-rate constraint was selected such that the temperatures in the stagnation regions would not exceed the capabilities of current passive TPS materials. This heating rate is held constant until the guidance algorithm determines that the roll angle is sufficient to allow the vehicle to reach the desired landing site. At this point, the excess range capability has been reduced to a level where holding the roll angle constant will allow the vehicle to reach the landing site with some margin. When the vehicle heading angle is pointed directly toward the landing site, the roll angle is reduced to zero in order to maximize the range. This strategy is consistent with that used for the current Space Shuttle Orbiter. Similar to the Shuttle, the maximum-crossrange entry was selected as the TPS design trajectory since it requires the vehicle to maintain the maximum stagnation-heating-rate boundary for the longest time. Relative to other missions, this will require the deepest entry into the atmosphere at the highest velocities and produce the highest heating rates over the vehicle surface. In terms of TPS requirements, this will therefore be the most demanding entry.

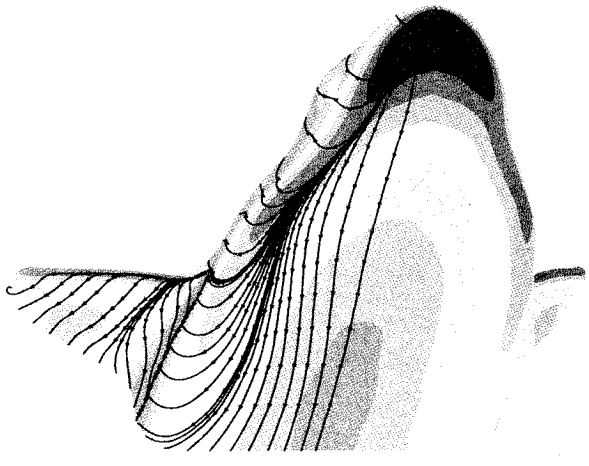

Fig. 7 HL-20 PLS perfect-gas CFD solution-streamline/heating pattern: Mach 6, angle-of-attack = 25 deg.

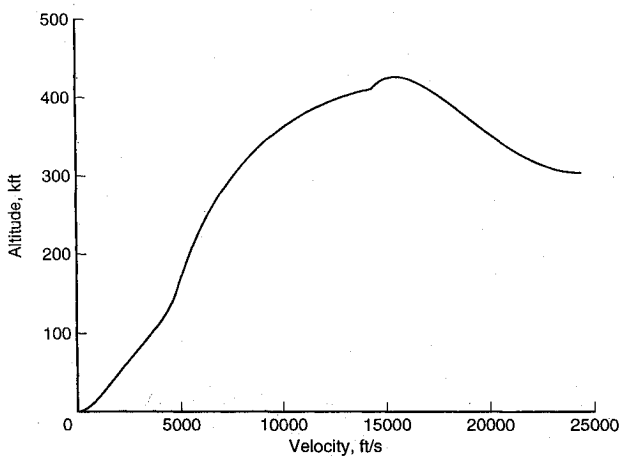

Fig. 8a Altitude-velocity profile for Titan III ascent into 50×100 n.mi., 28.5-deg orbit.

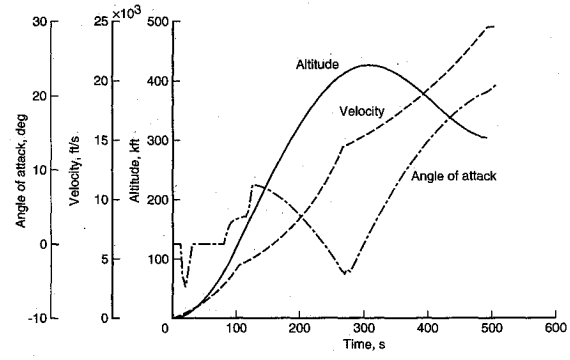

Fig. 8b Trajectory parameter time histories for Titan III ascent into 50×100 n.mi., 28.5-deg orbit.

For the HL-20, the nominal entry trajectory was developed assuming that the vehicle center of gravity (c.g.) was located at 55.5% of the body length. The trim angle-of-attack for undeflected control surfaces and this c.g. location was found to be 28.8 deg at hypersonic speeds.[2] An altitude-velocity profile along with time histories of several parameters are shown in Figs. 5a and 5b for the nominal trajectory. The reference heating rate selected was 90 Btu/ft^2-s with a corresponding crossrange of 1000 n.mi. By modifying the initial entry flight-path angle to change the timing of the pull-out, entries with stagnation heating rates of 95 and 85 Btu/ft^2-s were also investigated. The resulting crossranges for these entries were 1006 and 978 n.mi., respectively. By moving the c.g. aft to 56.5%, the entry trim angle-of-attack was increased to 34 deg. In addition, the maximum crossrange was reduced to about 860 n.mi. and the reference heating rate to 80 Btu/ft^2-s. Investigation of these parametrics simply demonstrated that the 90-Btu/ft^2-s, 1000-n.mi. entry previously chosen is very nearly optimum in terms of all the performance parameters.

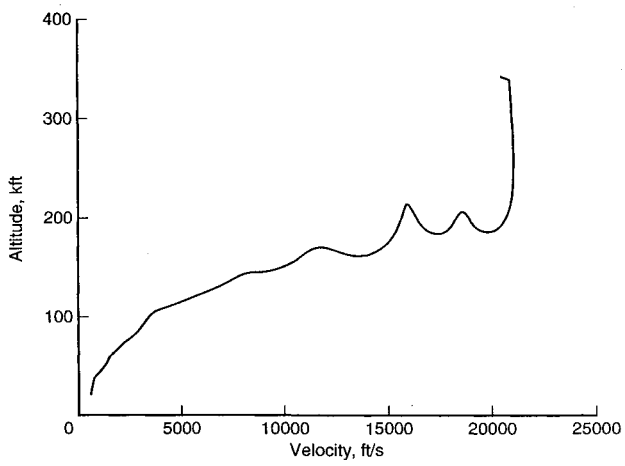

Fig. 9a Altitude-velocity profile for transatlantic abort: maximum heating case, abort at 430 s into ascent.

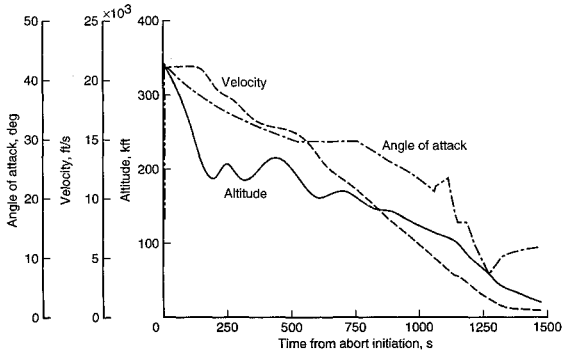

Fig. 9b Trajectory parameter time histories for transatlantic abort: maximum heating case, abort at 430 s into ascent.

Aerodynamic-Heating Analysis and Results

Stagnation Regions

A Fay and Riddell stagnation-point heating analysis[22] is used to determine the heating levels over the nosecap of the vehicle throughout the entry. The flight-regime selection parameter,[7] $M_\infty / z_e(Re_\infty)^{1/2}$, is used to determine whether a continuum, slip-flow (transitional) or free-molecular-flow calculation is performed at each trajectory point. For the current configuration and trajectory, a continuum calculation is performed for altitudes below 200 kft and Mach numbers below 16. In the low-density, low-Reynolds number, highly-viscous transitional regime above that, however, an increase in heating rates of approximately 25% over the continuum predictions occurs due to the effect of viscous interactions. Although the geometric nose radius in the symmetry plane of the vehicle at a 0-deg angle-of-attack is slightly less than 1 ft, the effective nose radius at angle of attack is significantly greater than this. A nosecap radius of 1.5 ft would limit the stagnation heating rate to 79 Btu/ft^2-s and the radiation equilibrium temperature to 3300°F, whereas a radius of 2.5 ft yields values of 58 Btu/ft^2-s and 3000°F, respectively. The effective nose radius of the HL-20 at a trim angle-of-attack of 28.8 deg was estimated to be 2.06 ft, corresponding to a heating rate of 64 Btu/ft^2-s and temperature of 3080°F. This radius represents an attempt to account for not only the angle-of-attack effects, but also the three-dimensional nose effects due to the nonspherical nature of the nosecap.

Wing-leading-edge heating rates are calculated using a simple swept-cylinder stagnation-line heating calculation based on a Fay and Riddell analysis with an empirical sweep effect.[7] The effective sweep angle used in the calculations is determined from the geometric sweep, together with the angle-of-attack and dihedral of the wing. The leading edges are assumed to be fully immersed in the freestream flow. This should yield a conservative, i.e., high, prediction for the heating rates, in contrast with the levels that would occur if the wings were assumed to be entirely engulfed within the bow shock. A determination of the flow regime, continuum or otherwise, is made similar to that for the stagnation-point calculation. Continuum flow dominates for altitudes below 120–130 kft and Mach numbers below 5–6, depending on the leading-edge radius. A radius of 0.5 in. results in a peak heating rate of 73 Btu/ft^2-s and a corresponding radiation equilibrium temperature of 3220°F, whereas a radius of 1.0 in. reduces the heating rate to 54 Btu/ft^2-s and a temperature of 2950°F. A radius of 1.0 in. was therefore selected based on the multi-use temperature capability of Advanced Carbon-Carbon (ACC). If we assume no bow-shock impingement, the wing-leading-edge heating rates will generally track those found at the stagnation point shown in Fig. 1. This issue remains a concern even though wind-tunnel flow visualization tests have shown no impingement on the vehicle surface to date. Recent equilibrium-air CFD solutions[4] obtained with LAURA at a Mach 15.8 flight condition at 180 kft and 25-deg angle-of-attack, however, indicate a possible impingement site near the tip of each wing surface. Figure 6, reproduced from Ref. 4, illustrates this, the dark spot at the tip of the wing leading edge indicating a small area of increased heating. Note that the wind-tunnel studies, as well as the CFD solutions that do not show evidence of this impingement, are based on perfect-gas conditions. This latest CFD solution is an equilibrium analysis that accounts for the real-gas effects likely in the actual flight environment. Further study will be required to address this issue. It must be determined whether the current TPS design for the leading edges will be sufficient to handle such an impingement or, if not, whether some trajectory shaping may be necessary in order to prevent its occurrence. Similarly, wing-shock interference effects must also be addressed. Figure 7 illustrates the flowfield calculated using LAURA for a Mach 6, 25-deg angle-of-attack, $Re_\infty = 2.3 \times 10^6$/ft wind-tunnel condition (perfect gas). The dark spot near the root of the wing appears to indicate an area of higher heating due to wing-shock interference. The heating level is roughly half that in the nose stagnation region, however, and thus no heating problems are anticipated in this area.

The entry profile used to generate the stagnation-heating rate shown in Fig. 1 is for an assumed 55.5% c.g. location, with pull-out on the 90-Btu/ft^2-s boundary (reference heating) described previously. The stagnation heating rate has a double peak at 63 Btu/ft^2-s (3060°F) initially as the guidance commands the vehicle to roll at pull-out. Since it takes a finite amount of time to roll, the vehicle pulls up slightly, then plunges back to the boundary. As the velocity and altitude decrease, the vehicle moves rapidly off the high heating rate. Just after 850 s into the entry, the vehicle unrolls as the heading reaches that of the landing site and causes the vehicle to climb for a short time (Fig. 5b). As the velocity continues to decrease, the stagnation-heating rate also decreases significantly.

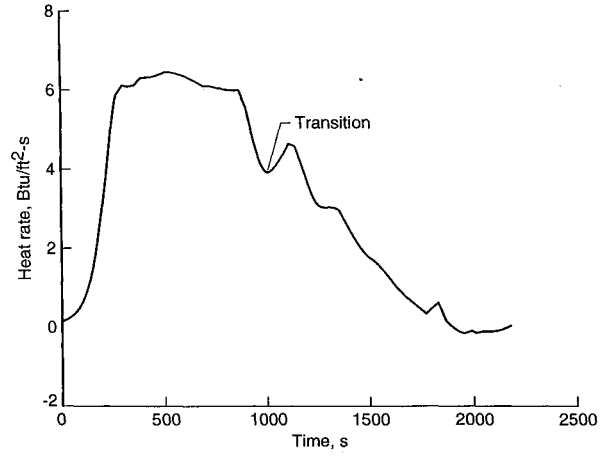

Fig. 10 Typical HL-20 PLS centerline entry heating-rate time history: $x/L = 1.0$.

At about 1000 s after entry interface (400 kft), the vehicle once again begins to plunge further into the atmosphere causing a temporary rise in the stagnation-heating rate. At about 1200 s, the angle-of-attack begins to decrease and the heating rate holds constant for a short period of time, followed by a steady decrease to landing.

The ascent stagnation-heating-rate profile shown in Fig. 1 represents a Titan III launch vehicle ascent. The associated trajectory parameters are illustrated in Figs. 8a and 8b. The peak stagnation-point heating, 14 Btu/ft^2-s (1960°F), occurs as the Titan reaches burn-out at about 500 s. The vehicle is at just over 300 kft and has accelerated to orbital speed. After the Titan is shutdown, the HL-20 coasts to a higher altitude before circularization. During this coast period, the heating rate decreases until the vehicle exits the atmosphere.

The most severe abort case, in terms of stagnation-point heating rate, occurs just as the transatlantic abort site comes within the entry range of the vehicle. The trajectory parameters for the entry from abort are shown in Figs. 9a and 9b. At this point in the ascent, the vehicle has reached almost 350 kft of altitude and about 22 kft/s in velocity. This altitude is too high to provide any significant lift and therefore the vehicle begins to plunge into the atmosphere when the thrust component is removed. The vehicle pulls up several times as the dynamic pressure builds up and the lift is sufficient to reverse the sign of the flight-path angle. A peak heating pulse of 78 Btu/ft^2-s, corresponding to a radiation equilibrium temperature of just under 3300°F, occurs at the first pull-up maneuver. That pulse is followed by progressively lower heating-rate peaks corresponding to each of the two subsequent pull-up maneuvers (see Fig. 1) and finally a steady decrease in heating until the landing site is reached.

Windward Surfaces

The analysis of the stagnation-region heating establishes the general level of heating for the entire vehicle. MINIVER is then used to extend the analysis to other critical regions of the vehicle. The Eckert-reference-enthalpy[23] approach, coupled with a Blasius flat-plate skin-friction solution[13] for laminar flow and the Schultz-Grunow[24] skin-friction relation for turbulent flow, is used in conjunction with the Mangler transformation[13] to determine heating along the windward centerline and the windward surface of the wings throughout the entry. Based on values extrapolated from Space Shuttle flight data,[16] transition criteria of $Re_\theta/M_e = 335$ for transition onset and 415 for a fully turbulent boundary layer are applied in the analysis of the windward surfaces. The assumptions for the prediction of the windward surface heating discussed in a previous section include a blunt-body flowfield and no crossflow effects. The CFD solution shown in Fig. 7 illustrates the flowfield calculated using the LAURA code for a Mach 6, 25-deg angle-of-attack, $Re_\infty = 2.3 \times 10^6$ wind-tunnel condition (perfect gas). The flowfield is remarkably similar to that demonstrated by the oil flow in Fig. 4 for a similar condition. Once again, little crossflow is apparent.

The entry heating-rate time history in Fig. 10 illustrates that even at the aft end of the vehicle where turbulent heating is most likely to occur, the flow remains laminar until late in the entry, approximately 1000 s, and that the transitional heating rate at that time remains significantly less than the preceding laminar values. An extremely conservative value for the onset of transition, $Re_\theta/M_e = 150$, was also examined. However, the conclusion that the laminar heating will dominate the heating environment for this relatively short vehicle remained the same. This is an important conclusion as previous studies[25] have shown a large TPS weight penalty associated with failure to maintain laminar flow throughout the high-heating phases of the entry.

Figure 11 shows the peak heating rates and corresponding radiation equilibrium temperatures that occur throughout the entry for each point along the windward centerline of the HL-20. Note that this figure does not represent a single flight condition, but rather the peak heating condition that each point on the vehicle experiences throughout the entire entry. It is apparent from the steady decrease in heating toward the aft end of the vehicle that, for all points on the windward centerline, the peak heating condition is laminar. Peak equilibrium heating generally occurs at about a Mach number of 24, an altitude of 230 kft, and 28.8-deg angle-of-attack. The maximum multiple-use temperatures for the Shuttle TPS, HRSI tiles (2500°F), and the ACC (3000°F) are indicated in Fig. 11, as is the single-use limit for the ACC (3300°F). The nose region of the HL-20 would require ACC, but most of the windward centerline is well below the limit for HRSI or HTP tiles[26] presently considered. Since there is a significant temperature margin, any deficiencies in the blunt-body/crossflow assumptions are not likely to impact the TPS selections made in this study. The windward-wing-surface heating rates were less than the windward centerline values at the same chordwise location. A conservative estimate of the heating to the windward wing/fin surface can be inferred from Fig. 11 by taking the heating rates at a given chordwise location to be approximately 70% of those on the centerline at the corresponding x/L locations.

Although previous heating studies including, but not limited to those in Refs. 9–11, have demonstrated the excellent agreement that may be obtained when comparing MINIVER results with flight- and wind-tunnel-test data, as well as benchmark CFD solutions, it was felt that verification of that trend for the HL-20 configuration would be an important contribution to this study. Figure 12 compares the laminar and turbulent heating rates predicted using MINIVER to wind-tunnel results obtained on the HL-20 configuration at a 25-deg angle-of-attack in air at Mach 6 and a Reynolds number of 8×10^6/ft (Ref. 6). The wind-tunnel data were obtained using two different techniques. The first is a standard phase-change technique, whereby the model is coated with a paint that melts at a known temperature. The length of time it takes the paint

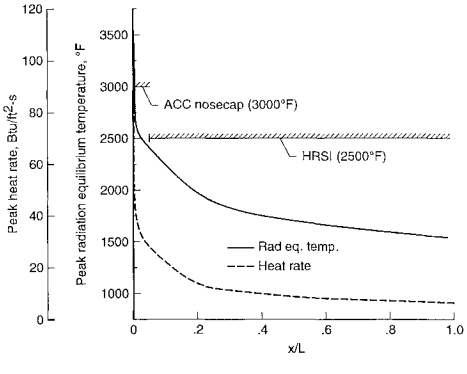

Fig. 11 HL-20 PLS windward centerline peak heating distribution/material requirements: Design entry trajectory, $\varepsilon = 0.85$, transition $Re_\theta/M_e = 335$.

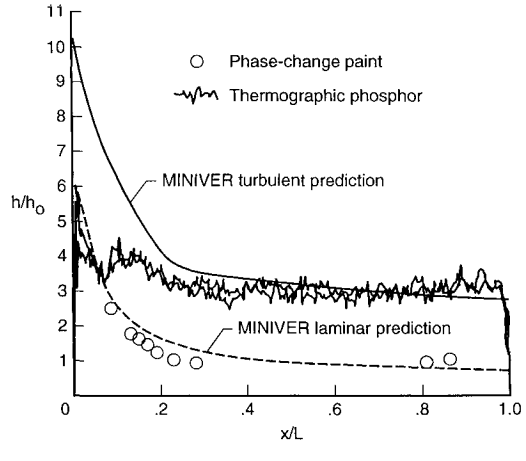

Fig. 12 Comparison of experimental results with engineering predictions for HL-20 PLS windward centerline heat-transfer distribution: Mach 6 air, angle-of-attack = 25 deg, $Re_\infty = 8.0 \times 10^6$/ft.

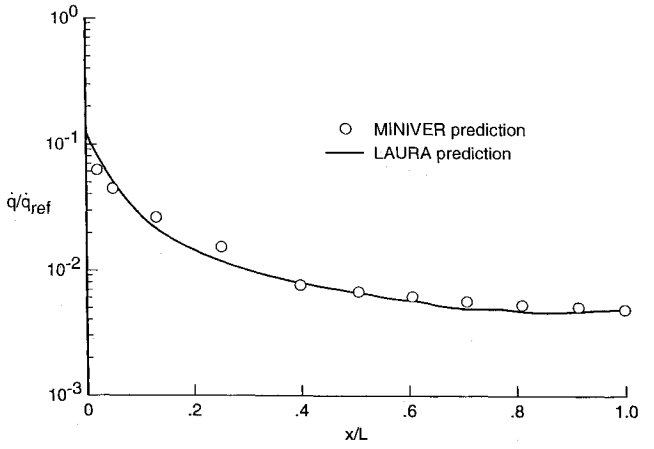

Fig. 13 Comparison of CFD and engineering solution for HL-20 PLS windward centerline heat-transfer distribution: Perfect gas, Mach 5.932 air, angle-of-attack = 25 deg, $Re_\infty = 2.3 \times 10^6$/ft.

to melt is an indication of the heating rate at each position on the vehicle. The second method is a thermographic phosphor technique, whereby the model is coated with a special paint whose spectral emissions change at specific temperatures. Reference 6 describes the wind-tunnel-test techniques and data in detail. The MINIVER laminar predictions presented in Fig. 12 show good agreement with the phase-change paint data, whereas the MINIVER turbulent predictions show good agreement with the thermographic-phosphor data. At a Reynolds number of 2×10^6/ft, Ref. 6 shows the thermographic-phosphor and phase-change paint data to be in good agreement. It is apparent that the boundary layer was somehow tripped during the thermographic phosphor tests at the higher Reynolds number. Whether this is due to an inherent roughness of the phosphor paint or some other effect is not known at this time. However, Ref. 6 does indicate that this result was repeatable.

Figure 13 illustrates a typical comparison between the MINIVER heating-rate predictions made along the windward centerline and the CFD prediction previously illustrated qualitatively in Fig. 7 for a lower Reynolds number case (Mach 6, 25-deg angle-of-attack, $Re_\infty = 2.3 \times 10^6$/ft wind-tunnel condition). The solid line represents results obtained using LAURA, whereas the circles represent predicted results from MINIVER. Excellent agreement is noted. This is a perfect-gas prediction but, nonetheless, lends credence to the MINIVER predictions being made at flight conditions. Efforts are underway to make comparisons for the Mach 15.8 flight condition illustrated in Fig. 6. The quantitative results presented in Ref. 4 for this condition were not available in time for inclusion in this portion of this study. It is hoped that more CFD solutions can be obtained for comparison with the MINIVER code at critical flight conditions, and these results should provide confidence in the engineering predictions until such time as flight-test data become available.

In addition to the phase-change and thermographic-phosphor tests already described, infrared images of the HL-20 have also been obtained.[15] Each of these techniques also gives one a qualitative look at the heating distribution on the vehicle. The qualitative results indicate that higher heating occurs not only on the nose cap and wing leading edges, but also near the edges of the windward surface (chines).

Leeward Surfaces

The heating to the leeward surfaces of the HL-20 vehicle was assumed to be relatively insignificant. At the hypersonic trim angle-of-attack where the highest heating levels occur, 28.8 deg, the entire leeward surface is shielded from the flow. The leeside heating calculations are performed utilizing an empirical correlation derived from Space Shuttle experience and developed by Bertin and Goodrich.[27] Similar to that of the Shuttle Orbiter, most of the leeward surface of the HL-20 configuration will be in a separated flow regime. Bertin and Goodrich's correlation is used only to determine qualitatively the heating levels over the leeward surface of the HL-20. The results suggest that the temperatures on the leeward surfaces would not exceed 800°F, well within the capability of current Shuttle blanket materials. Possible flow reattachment and vortical flow "scrubbing" on the leeward surfaces may result in local "hot spots," however. Phase-change paint tests[6] do indicate some increase in heating on the canopy due to flow separation and reattachment, but only at the low angles-of-attack that occur late in the entry when heating is no longer an issue. Further investigation into potential leeward surface heating problems due to flow separation, reattachment, and vortical "scrubbing" of the leeward surfaces should be addressed in the future with tests in real-gas facilities or through further CFD solutions. No heating calculations were performed on the vertical tail. It is relatively small and is presumed to be out of the freestream flow until very low angle-of-attacks and supersonic Mach numbers are reached. Similar to the canopy heating situation, heating is not thought to be an issue at these flight conditions.

Thermal Protection System Selection

The TPS selection for the HL-20 vehicle is made with four primary goals in mind. First, it must protect the vehicle structure and crew from the aerothermal environment to which the vehicle will be subjected. It must be reusable with minimal maintenance requirements. It should be highly durable, i.e., capable of withstanding not only the hazards related to the space environment such as micro-meteoroid impact, but also those associated with ground handling and weather conditions. Finally, the HL-20 TPS must utilize near-term technology. As indicated in a previous section, the two aerothermodynamic parameters driving the TPS design are the 1) peak heating rates/temperatures and 2) total heat load. The first condition determines the materials that can be utilized based on maximum temperature capabilities, and the second determines the amount of TPS that will be required to insulate the vehicle. This study addresses only the first issue. Greater depth of analysis will be necessary in order to "size" the TPS, i.e., determine the TPS/insulation distribution over the entire vehicle. For the purposes of this investigation, the radiation equilibrium temperatures that have previously been presented are assumed to be the vehicle surface temperatures and are used for the selection of the thermal protection materials/systems. These calculations assume a surface with an emissivity of 0.85 and no thermal mass. The assumption of zero thermal mass should yield a slightly conservative estimate of the TPS requirements. In reality, a certain amount of the incident heat will be stored in both the TPS and structure, and the surface temperatures will be somewhat lower than the radiation equilibrium values calculated.

The Rockwell concept[28] uses a graphite/polyimide heatshield structure with a maximum temperature capability of 550°F, whereas the Lockheed concept[29] utilizes a titanium structure with a maximum temperature capability of 1000°F. Although the increased temperature capability of these structural materials may reduce external TPS requirements when compared to those for a 350°F aluminum structure, it would also necessitate the use of more internal insulation to isolate the crew cabin and avionics. This requirement would partially negate the advantage that might be gained through the increased temperature capabilities of the structure. HTP tiles[26] are used on the windward surfaces in the Rockwell concept, with a direct bond of the HTP tiles to the graphite/polyimide structure assumed. The similarity in thermal expansion coefficients between the tiles and structural material minimizes the thermal stresses. The Lockheed concept also utilizes HTP tiles on the windward surfaces, except with direct bonding to the titanium structure. Both concepts employ a "warm" wing-structure concept. The Rockwell concept assumes a graphite/polyimide wing. As noted in a previous section, the leeward surface of the wing is expected to experience temperatures less than 800°F and, therefore, little external TPS would be required for any of the concepts. However, due to the uncertainties in the flow in this leeside region, some TPS such as an AFRSI blanket may be advisable on the upper surfaces of the wing.

The Reinforced Carbon-Carbon nose and wing leading edges on the Space Shuttle have demonstrated surprising durability. A stronger carbon-carbon material, ACC, is now available and used commercially. This material has very high strength at high temperatures, but is dependent on a silica coating to protect it from oxidation. For the purposes of this study, the temperature limits for the ACC have been assumed to be 3000°F for multiple uses and 3300°F for a single use. Results described previously have indicated that, for a nominal hypersonic trim angle-of-attack of 28.8 deg and leading-edge radius of at least 1 in., the peak radiation equilibrium temperatures on the nosecap and leading edges will be on the order of 3000°F. As noted previously, a slight increase in effective nose radius from the current value (2.06 ft) to 2.5 ft will ensure temperatures below the ACC multi-use capability. Results based on predictions made using hypersonic impact theory show that increased nose blunting, if necessary, would not significantly degrade the vehicle's hypersonic aerodynamic performance. Further investigation will be required to determine the effect at subsonic conditions. Based on this discussion, ACC is therefore selected for the TPS in these regions. It has also been noted that phase-change paint tests and infra-red studies indicate the heating levels on the chines to be of roughly the same order. ACC is therefore suggested for this area as well. The single-use capability of this material (3000°F) is also sufficient for the abort case.

Reusable surface insulation tiles have been a key to the Shuttle Orbiter's ability to perform mission after mission in the high entry-heating environment. The current HRSI tile system with a multi-use capability to 2500°F continues to require considerable maintenance between flights, although this effort has been reduced significantly over the years. The relatively small scale of the HL-20 vehicle alone will reduce this problem significantly. In addition, several organizations have devoted considerable effort toward improvement in tile durability. More recent efforts have produced the HTP, FRCI-12, and AETB-8 and AETB-12 (alumina-enhanced thermal barrier) tiles. These tiles are described in more detail in Ref. 30. Each of these tiles exhibits improved strength and reduced weight characteristics relative to the comparable Shuttle system with no sacrifice in temperature capability. As shown in Figs. 3 and 11, HRSI is chosen for the windward, nonstagnation regions of the HL-20 vehicle aft of approximately the 8% body location, including the windward wing surface aft of the leading edge. However, replacement of the HRSI with any of the tiles mentioned here is suggested once flight certification is given to these tiles. For the lower heating regions of the leeward and side surfaces, AFRSI, which is currently used on the Shuttle leeward surfaces, is chosen. This is a flexible blanket insulation with a multi-use temperature capability of 1200°F. Several other blanket systems are currently available. They include Tailorable Advanced Blanket Insulation and Composite Flexible Blanket Insulation, each of which could be utilized on the leeward surface of the HL-20. Reference 30 presents the results of an analysis of these tiles and blankets for application to the HL-20 PLS concept. Figure 3 illustrates the TPS layout for the surface of the HL-20 vehicle, utilizing only TPS found on the current Shuttle Orbiter. Each of the systems identified in this section could be employed successfully. The questions that remain to be answered are which systems can demonstrate the greatest durability, be the easiest to repair and/or maintain in the field and, ultimately, the most cost-effective.

Concluding Remarks

This article has described the methods that have been used to predict the aerothermal environment and make the TPS selection for the HL-20 PLS vehicle. Analytical techniques ranging from simple engineering ones to CFD solutions have been utilized. The unique integration of these analytical predictions with the results of extensive wind-tunnel tests has been described. The abort, ascent, and entry trajectories were investigated and the entry environment was demonstrated to represent the design case for the TPS for this vehicle. The aerothermal environment for several critical regions of the vehicle, including the stagnation areas of the nose and leading edges, the windward centerline, chines, and wing surfaces, and the leeward surfaces of the fuselage, wings, and vertical tail, has been described. Laminar heating has been shown to dominate and peak temperatures to be well within the capabilities of current TPS/materials technology. Comparisons of engineering predictions with CFD solutions, as well as wind-tunnel-test results, have shown very good agreement and demonstrated the validity of the engineering approach. A TPS based on current technology has been selected for the HL-20 PLS vehicle. ACC was chosen for the stagnation areas of the nosecap, leading edges, and chines. The Shuttle HRSI was selected for use over the windward surfaces away from the stagnation areas, and AFRSI for the leeward surfaces. Several recently developed TPS concepts that have potential for improved durability without degradation of temperature capabilities have also been identified.

References

[1]Stone, H. W., and Piland, W. M., "21st Century Space Transportation System Design Approach: HL-20 Personnel Launch System," *Journal of Spacecraft and Rockets,* Vol. 30, No. 5, 1993, pp. 521–528.

[2]Ware, G. M., and Cruz, C. I., "Aerodynamic Characteristics of the HL-20," *Journal of Spacecraft and Rockets,* Vol. 30, No. 5, 1993, pp. 529–536.

[3]Naftel, J. C., and Talay, T. A., "Ascent Abort Capability for the HL-20," *Journal of Spacecraft and Rockets,* Vol. 30, No. 5, 1993, pp. 628–634.

[4]Weilmuenster, K. J., and Greene, F. A., "HL-20 CFD Analysis," *Journal of Spacecraft and Rockets,* Vol. 30, No. 5, 1993, pp. 558–566.

[5]Powell, R. W., "Six-Degree-of-Freedom Guidance and Control-Entry Analysis of the HL-20," *Journal of Spacecraft and Rockets,* Vol. 30, No. 5, 1993, pp. 537–542.

[6]Horvath, T. J., Rhode, M. N., and Buck, G. M., "Aerothermodynamic Measurements on a Proposed Assured Crew Return Vehicle (ACRV) Lifting Body Configuration at Mach 6 and 10 in Air," AIAA Paper 90-1744, June 1990.

[7]Engel, C. D., and Praharaj, S. C., "MINIVER Upgrade for the AVID System, Vol. I: LANMIN User's Manual," NASA CR-172212, Aug. 1983.

[8]Gnoffo, P. A., "Upwind-Biased Point-Implicit Relaxation Strategies for Viscous Hypersonic Flows," AIAA Paper 89-1972, June 1989.

[9]Thompson, R. A., "Comparison of Nonequilibrium Viscous-Shock-Layer Solutions with Shuttle Heating Measurements," *Journal of Spacecraft and Rockets,* Vol. 27, No. 2, 1990, pp. 162–169.

[10]Wurster, K. E., Zoby, E. V., and Thompson, R. A., "Flowfield and Vehicle Parameter Influence on Results of Engineering Aerothermal Methods," *Journal of Spacecraft and Rockets,* Vol. 28, No. 1, 1991, pp. 16–22.

[11]Wurster, K. E., and Zoby, E. V., "An Experimental Heat Transfer Investigation of an Advanced Winged Entry Vehicle at Mach 10," AIAA Paper 83-0409, Jan. 1983.

[12]Baranowski, L. C., "Influence of Cross-Flow on Windward Centerline Heating," McDonnell Douglas Astronautics Co., Rept. MDC E0535, St. Louis, MO, Dec. 1971.

[13]Schlichting, H., *Boundary Layer Theory,* 6th English ed., McGraw-Hill, New York, 1968.

[14]Brauer, G. L., Cornick, D. E., and Stevenson, T., "Capabilities and Applications of the Program to Optimize Simulated Trajectories (POST)," NASA CR-2770, Feb. 1977.

[15]Freeman, D. C., Jr., "HL-20 Personnel Launch System—A Concept Definition Case Study," IAF Paper 92-0856, Sept. 1992.

[16]Goodrich, W. D., Derry, S. M., and Bertin, J. J., "Shuttle Orbiter Boundary Layer Transition at Flight and Wind Tunnel Conditions," *Shuttle Performance: Lessons Learned,* NASA CP-2283, Part 2, March 1983, pp. 753–779.

[17]Shideler, J. L., "Predicted and Tested Performance of Durable TPS," *Current Technology for Thermal Protection Systems,* NASA CP-3157, Feb. 1992, pp. 97–129.

[18]U.S. Standard Atmosphere, National Oceanic and Atmospheric Administration, NASA and U.S. Air Force, Washington, DC, Oct. 1976.

[19]Hansen, C. F., "Approximations for the Thermodynamic and Transport Properties of High Temperature Air," NASA TR R-50, 1959.

[20]Korobkin, I., and Hastings, S., "Mollier Chart for Air in Dissociated Equilibrium at Temperatures of 2000°K to 15000°K," NAVORD Rept. 4446, May 1957.

[21]Chapman, D. R., "An Approximate Analytical Method for Studying Entry into Planetary Atmospheres," NASA TR R-11, 1959.

[22]Fay, J. A., and Riddell, F. R., "Theory of Stagnation-Point Heat Transfer in Dissociated Air," *Journal of Aerospace Sciences,* Vol. 25, No. 2, 1958, pp. 73–85, 121.

[23]Eckert, E. R. G., "Survey on Heat Transfer at High Speeds," ARL 189, U.S. Air Force, Dec. 1961.

[24]Schultz-Grunow, F., "A New Resistance Law for Smooth Plates,"

Luftfahrforschung, Vol. 17, 1940, pp. 239–246 (translation); also NACA TM 986, Sept. 1941.

[25]Wurster, K. E., "An Assessment of the Impact of Transition on Advanced Winged Entry Vehicle TPS Mass," AIAA Paper 81-1090, June 1981.

[26]Banas, R. P., Creedon, J. F., and Cunnington, G. R., Jr., "Thermophysical and Mechanical Properties of the HTP Family of Rigid Ceramic Insulation Materials," AIAA Paper 85-1055, June 1985.

[27]Bertin, J. J., and Goodrich, W. E., "Effects of Surface Temperature and Reynolds Number on Leeward Shuttle Heating," *Journal of Spacecraft and Rockets*, Vol. 13, No. 8, 1976, pp. 473–480.

[28]Ehrlich, C., "HL-20 Concept: Design Rationale and Approach," *Journal of Spacecraft and Rockets*, Vol. 30, No. 5, 1993, pp. 573–581.

[29]Urie, D. M., Floreck, P. A., McMorris, J. A., Elvin, J. D., "Design for Effective Development and Prototyping of the HL-20 Concept," *Journal of Spacecraft and Rockets*, Vol. 30, No. 5, 1993, pp. 582–589.

[30]Chiu, S. A., and Pitts, W. C., "Reusable Surface Insulations for Reentry Spacecraft," AIAA Paper 91-0695, Jan. 1991.